Experimental and kinetic study on the laminar burning speed, Markstein length and cellular instability of oxygenated fuels

Qiao Wang[1], Wanchen Sun[1], Liang Guo[1*], Shaodian Lin[1], Peng Cheng[1], Hao Zhang[1], Yuying Yan[2]

1. Jilin University State Key Laboratory of Automotive Simulation and Control, Changchun 130025, China

2. Faculty of Engineering, University of Nottingham, Nottingham, UK, NG7 2RD

*Corresponding author: Liang Guo; Email: liangguo@jlu.edu.cn

Abstract: The laminar burning speed, Markstein length and cellular instability of three oxygenated fuels, polyoxymethylene dimethyl ether 3 (PODE$_3$), dimethyl carbonate (DMC) and n-butanol (NB), were experimentally studied using spherical flame propagation method. Both of the three fuels are potential alternatives for petrochemical gasoline and diesel. Laminar burning speeds and Markstein lengths were measured at ambient pressure and elevated temperature (363 K-423 K) with three extrapolation models including linear and non-linear employed to extract the unstretched flame speed. Onset of flame cellular instability of the three fuels was determined at high pressure (0.5-0.75 MPa) which was favored to the occurrence of cellular instability. Three well-validated mechanisms for PODE$_3$, DMC and NB respectively were used to numerically analyze the flame structure and then understand the underlying effect of the molecular structure of oxygenated fuels on laminar flame propagation. Results show that PODE$_3$ has the highest laminar burning speed among the three, supporting by both thermal effect and kinetic effect. While the laminar burning speed of NB is higher than that of DMC, which is due to the combined effect of thermal factor and kinetic factor. The molecular structure of oxygenated fuels exerts an influence on the laminar flame propagation through the fuel-specific cracking pathway and resulting formed intermediates with different reactivity. The absence of C-C bond within $PODE_3$ and DMC leads to the formation of substantial oxy-intermediates (CH_2O) with high reactivity during fuel decomposition. $PODE_3$ has the most stable flame among the three because of the strong stretching of $PODE_3$ flame. The flame stability of DMC and NB is approximately similar especially at high initial pressure.

Keywords: Oxygenated fuel; Laminar burning speed; Markstein length; Cellular instability.

1. Introduction

Transport sector accounts for about 20% of global primary energy consumption and 23% of carbon dioxide (CO_2) emission [1], which is an important source of energy consumption and environmental pollution. Therefore, the limits of vehicle emission regulations and fuel consumption regulations are constantly tightened all over the world. In response, automobile manufacturers have to develop new technologies to continuously improve the efficiency of energy utilization and reduce pollutant emissions, and fuel companies have to actively develop renewable alternative fuels to reduce dependence on non-renewable fossil energy [2,3].

Oxygenated fuel is a kind of fuel with oxygen atom in the molecular structure, which has been proved to be beneficial to engine emissions, especially unburned HC and particulate matters [4,5]. Some oxygenated fuels, such as methanol and ethanol, have been commercialized. Many oxygenated fuels under study have been preliminarily proved to be potentially alternative fuels for vehicles through comprehensively considering their production, operation, compatibility with existing automotive technologies and environmental friendliness, etc. n-butanol (NB), dimethyl carbonate (DMC) and polyoxymethylene dimethyl ether 3 ($PODE_3$) are three of these oxygenates, which are also the object of present study because they represent three kinds of oxygenated fuel with different functional groups, namely alcohol group, ester group and ether group respectively. Main chemical properties of PODE$_3$, DMC and NB are presented in Table 1. The synthesis technology and industrial production of these three fuels are constantly improving, which greatly promotes their application as alternative fuels [6-8]. In the past few years, some studies have confirmed that they can be used as pure fuel or oxygenated additive to improve the combustion, emission and performance of spark ignition (SI) engine, compression ignition (CI) engine or dual-fuel engine [9-14]. In particular, the absence of C-C bond in DMC and PODE$_3$ has become a favorable characteristic for improving engine emission [15,16].

Table 1 Main chemical properties of PODE$_3$, DMC and NB

	PODE$_3$	DMC	NB
Molecular structure	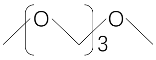	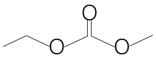	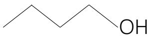
Chemical formula	$C_5H_{12}O_4$	C3H6O3	C4H10O
Mole weight (g/mol)	136.14	90.08	74.12
C/H ratio	0.42	0.5	0.4
Oxygen content（wt%）	47.1	53.3	21.6
Lower heating value (MJ/Kg)	19.14	15.78	33.1
Stoichiometric ratio	6.06	4.57	11.21

It is preferable to study systematically on the fundamental combustion characteristics and chemical kinetics of combustible mixtures before developing combustion technologies. The laminar flame characteristics, including laminar burning speed, Markstein length and flame instability, are important for understanding the combustion mechanism of fuel/oxidizer mixture [17]. They are also helpful to describe various practical combustion phenomena, such as flame stabilization, flame flashback, flame blowout and flame extinction [18]. Laminar burning speed is one of the most important physicochemical parameters of the combustible mixture, which is always used to validate the kinetic modeling. It is well recognized that laminar burning speed is directly related to the thermodynamic conditions of combustible mixture and fuel chemistry. Therefore, it is expected that fuel molecular structure has an effect on the laminar flame propagation. In fact, previous investigations have already given valuable insight into the impact of fuel structure in spite of focusing mainly on hydrocarbons [19-23]. Results show that the laminar burning speeds of C_5-C_{12} n-alkane are nearly identical [20,21], which suggests the dominant fuel oxidation mechanism and molecular transports are similar for these n-alkane fuels. The reason for this fuel similarity has been attributed to that these n-alkanes have similar straight-chain fuel structure and follow the similar pathway to decompose into similar intermediate fragments which govern the flame propagation. Wu et al. [24] has expended the general rule for hydrocarbons to alcohols by experimentally and kinetically compared the laminar burning speed of butanol isomers. He commented that this generality is due to the C-O, O-H bonds in alcohols that have similar bond energy as that of C-C and C-H bond. Consequently, the role of an O atom is similar to a C atom when considering the extent of branching of a fuel. As for $PODE_3$ and DMC, since there is no C-C bond within the fuel structure but only C-O bond, it behooves us to examine the effect of the molecular structure of $PODE_3$ and DMC on the flame structure and resulting flame propagation. It is of interest to study if the C-O bonds in $PODE_3$ and DMC act as the C-C when participating in oxidization reaction. If this indeed holds, this could lead to potential generalization and simplification in the description of the oxidation and flame processes of these fuels.

Premixed laminar flame is instinctively subjected to instability even without external disturbance

[25]. Cellular structures formed on the flame front increase the flame surface area and cause flame self-acceleration [26]. In this regard, Markstein length and cellular instability for various fuel/oxidizer mixtures have been studied extensively [27-31]. Laminar flame characteristics of butanol have been widely studied by various methods of experimental measurement and mechanism prediction [24,32,33]. However, these studies for $PODE_3$ and DMC are limited, which is far behind their application researches in actual combustion devices. Sun et al. [34] measured the laminar burning speed of $PODE_3$/air mixture at atmospheric pressure and initial temperature of 408 K using outwardly spherical flame method, which was used to validate their high temperature reaction mechanism of $PODE_{1-3}$. In fact, this is the only experimental determination of the laminar burning speed of $PODE_3$ at present. While, the research on the flame propagation and cellular instability of $PODE_3$ have not been done. As for DMC, Bardin er al. [35] measured the laminar burning speed of DMC/air mixture at unburned gas temperature up to 358 K. Yu et al. [36] studied the laminar flame characteristics of DMC using spherical propagation flame method. Laminar burning speed was measured at elevated temperature and pressure and the propensity of flame instability varying with initial pressure and equivalence ratio was evaluated. Atherley et al. [37] reported the latest research on DMC oxidation and pyrolysis. They measured the laminar flame speeds at an initial pressure of 1.013 bar, initial temperature of 318 K, 363 K, and 423 K for various equivalence ratios in a spherical vessel. The obtained data were compared to several detailed kinetics models from the literature.

The first aim of present study is to provide archival laminar burning speed for the three fuels, especially $PODE_3$ and DMC; the second is to examine the underlying effect of molecular structure of oxygenated fuel on the laminar flame propagation; the third is to compare the flame instability of the three fuels. In the following section the experimental procedure and data processing method will be described, then the numerical method along with the employed kinetic mechanisms are presented in section 3. Finally, both the measured and calculated laminar flame characteristics for the three oxygenates are presented and analyzed in section 4.

2. Experimental apparatus and data processing

2.1 Experimental apparatus

The measurements of laminar burning speed based on outwardly spherical flame were conducted in a closed stainless-steel constant volume combustion vessel. The interior of the vessel is cylindrical, with a diameter of 135 mm, a length of 136 mm and an internal volume of 1.95 L. The asymmetric effect of flame propagation caused by non-spherical volume can be weaken by almost equal diameter and length [38]. Two pairs of quartz window are arranged orthogonally. One pair provides optical channel for high-speed photography with diameter of 50 mm, and the other one provides optical channel for laser with diameter of 25 mm, which it is not used in current study. The thickness of all the quartz windows is 30mm and the material is JGS-1, which is safe enough to withstand the instantaneous high pressure produced by deflagration under the initial conditions of this study (T_u:363~423 K, P_u:0.1~0.75 MPa). Two ignition electrodes are arranged vertically in the center of the combustion vessel, which is different from the horizontal arrangement method in previous studies. Same arrangement was adopted in the study of Ossama M et al. [39]. An electric heater (1.5 kW) located outside the vessel is used to heat the mixture to specified initial temperature (up to 423 K). The ambient temperature (i.e. initial temperature) in the combustion vessel is measured by a K-type thermocouple located in the optical central, so as to minimize the thermal effect of the vessel wall. A PID controller is used to control the voltage of the heater, and the control accuracy of the initial temperature is ±1 K.

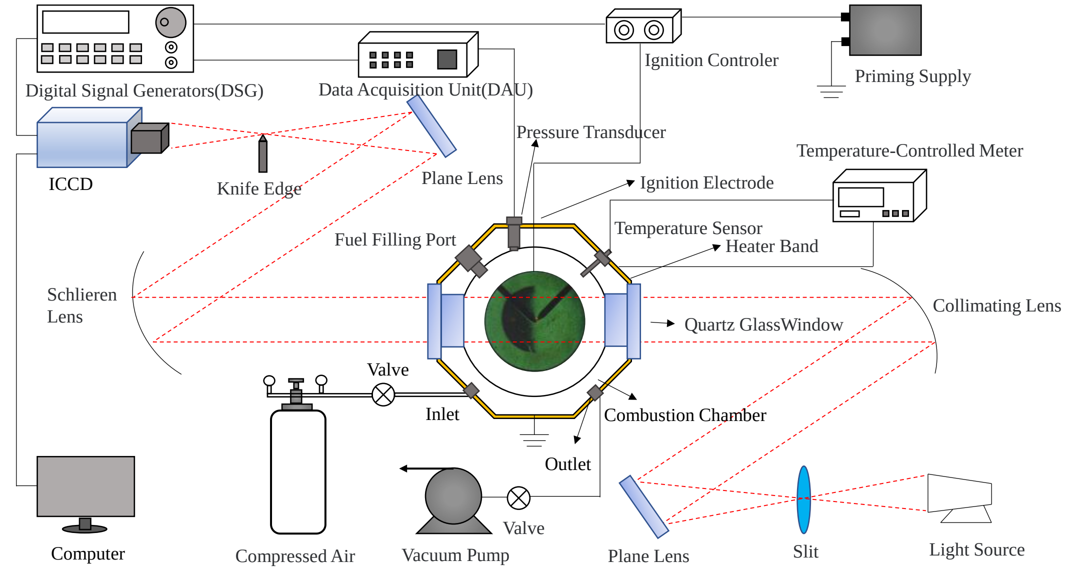

Fig.1. Schematic diagram of the experimental setup

The oxidizer used in the study is synthetic air composed of 21% O_2 and 79% N_2. Tested $PODE_3$ is provided by Shandong Chenxin new energy Co. Ltd. in China, with a purity of 91.27%. The mass fraction of each component within the tested PODE is shown in Table 2. Tested DMC and NB is provided by Aladdin Co., Ltd. with a purity higher than 98%. The mixture is prepared based on partial pressure method. Two types of pressure sensors are used to measure the pressure in the vessel, one is the diffusion silicon type which is used to measure the pressure during the mixture preparation, and the other is the piezoelectric type (Kistler 6052c) which is used to measure the pressure during the flame penetration. The injection volume of liquid fuel calculated according to partial pressure and fuel density is injected into the combustion vessel through a micro injector, the resolution of which is 1μm. There need about 10-15 minutes, according to the initial conditions, for injected fuel to evaporate and mixed sufficiently with the oxidizer (air) before being ignited. The mixed gases under each tested condition are checked with Gas Chromatography (GC) method to assure the specified equivalence ratio Φ was achieved. Then, the mixture is ignited, at the same time the high-speed photography is started to capture the schlieren image of flame propagation. Only one discharge per ignition and the duration is 10 μs. The gap between electrodes can be adjusted in the range of 0-5 mm, and the gap used in the test is 3 mm. In the process of flame propagation recorded by schlieren method, the LED cold light source is used for visualization. The light is processed by two plane mirrors and two spherical mirrors and captured by high-speed camera. As shown in Figure 1, the whole schlieren system is arranged in a "Z" shape. The focal length and diameter of two spherical mirrors (schlieren and collimator) are 1500 mm and 150 mm respectively. The high-speed camera is the phantom v611 series CMOS camera manufactured by Vision Research company of the United States. In this study, the shooting frequency is 10000 FPS, the exposure time is 100 μs, and the resolution is 800×600 pixels^2. Each mixture is tested three times in order to reduce the experimental error. After each test, the combustion vessel is completely evacuated with a vacuum pump, and then fresh air is used to clean the inner chamber of the vessel for many times to avoid the influence on the next test.

Table 2 Components of tested PODE

Component	Methyl formate	H_2O	$PODE_1$	$PODE_2$	$PODE_3$	$PODE_4$	The rest
Mass fraction (%)	0.05	0.05	0.04	0.19	91.27	8.09	0.31

2.2 Data processing

The instantaneous flame image recorded by the schlieren photography system is processed by a MATLAB code. The edge of propagating flamefront is detected with a self-developed algorithm. The equivalent radius (r_f) is deduced by calculating the area of the approximately spherical flame region. All the selected flame images are processed with the same method, and the flame radius time history ($r_f(t)$) is obtained finally.

When assuming that the combustion gas is stationary and the flame front is regarded as an infinitely thin surface, the starched flame propagation speed (S_b) is given by Eq. (1),

$$S_b = \frac{dr_f}{dt} \tag{2}$$

where r_f is flame radius and *t* is the flame propagating time from ignition. Local flow straining, flame curvature, and flame instability induce flame stretch which has significant effect on the determination for laminar burning speed and Markstein length [25]. Flame stretch is defined as logarithmic rate of change of flame area with time. For spherically stretched flame, the stretch rate K can be expressed by Eq. (2),

$$K = \frac{1}{A}\frac{dA}{dt} = \frac{2}{r_f}\frac{dr_f}{d_t} = 2\frac{S_b}{r_f} \tag{1}$$

where *A* represents an infinitesimal area of the flame surface. The range of flame radius should be selected rigorously for determining the laminar burning speed. That is because the spherical flames can go through an unsteady transition stage from an ignition kernel to a propagating front. The flame propagation is affected by ignition energy during the initial periods, while by the wall confinement during the final periods [40]. The cylindrical chamber boundary can also modify the flame propagation under large flame radius [38]. Lots of studies have been conducted to determine the optimal range of flame radius for calculating the flame speed more accurately [41,42]. Referred to the study of [38], the lower radius limit in present study is 6mm to remove the effect of the ignition, and the value for upper radius is 20 mm, less than 0.3 times of the wall radius.

In fact, almost all the practical flames and laboratorial flames used to measure the laminar flame characteristics suffer from stretch. That make the flame propagation modified by some factors, such as flame curvature, heterogeneous flow field, nonequidiffusion effect. Therefore, it is necessary to extrapolate the flame penetration speed to zero stretch in order to extract the unstretched flame speed and Markstein length. According to how quantitatively considering the effect of flame stretch, researchers have developed different extrapolation models to represent the relationship between flame propagation speed and flame stretch rate. All these models are derived from asymptotic analysis based on certain assumptions. The linear extrapolation model (LM) is given by Eq. (3),

LM	$S_b = S_b^0 - L_bK$	(3)

where S_b^0 is the unstretched flame propagating speed of burned gas and L_b is the Markstein length. It is based on the assumption that the Lewis number of the combustible mixture is close to 1 and the flame is weakly stretched. Therefore, it can be predicted that there is a certain degree of uncertainty when using this model for extrapolation. The nonlinear extrapolation model proposed by Kelley and Law [40] (NM1) is given by Eq. (4), that is, the unstretched flame speed changes nonlinearly with flame stretch. The model is based on quasi-steady state and weakly stretched flame penetration. It allows arbitrary combustible mixture and Lewis number. Obviously, the model is more general and has been widely used in recent years.

NM1	$(\frac{S_b}{S_b^0})^2\ln(\frac{S_b}{S_b^0})^2 = -2\frac{L_bK}{S_b^0}$	(4)

Considering the influence of strong stretching and general Lewis number, Chen et al. [43] proposed another nonlinear model within the limit of large flame radius. This model is given by Eq. (5) (NM2). It can be seen that there is a linear relationship between flame rate and flame curvature.

NM2	$\frac{S_b}{S_b^0} = 1 - 2\frac{L_b}{r_f}$	(5)

A lot of efforts have been devoted to improving the accuracy of extracting flame propagation speed from stretched flames. However, the selection of different extrapolation models has become an important source of uncertainty. The performance and accuracy of different extrapolation models for laminar burning speed and Markstein length measurements using a spherical expanding flame were compared [43,44]. The results show that the accuracy depends largely on the Lewis number of the mixture. In current study, the performance of the three most popular extrapolation models: LM, NM1 and NM2 in extracting the laminar burning speed and Markstein length of the three oxygenated fuels was compared. Detailed analysis was presented in *Supplementary Material*. It is noted that quantitatively evaluating the accuracy of three models is beyond the scope of this study. The flame speed data in *Result and Discussion section* is obtained consistently from extrapolation with NM1 which allows qualitatively comparison between different fuels. Lastly, once the unstretched flame propagating speed of burned gas is extracted, the laminar burning speed with respect to unburned gas can be determined based on the mass conservation on flame surface, as showed in Eq. (6), where ρ_b and ρ_u are the density of burned gas and unburned gas respectively.

$$S_u^0 = S_b^0 \ (\rho_b/\rho_u) \tag{6}$$

3 Numerical simulation

In this study, the PODE$_3$ mechanism of Sun et al. [34], DMC mechanism of Alexandrino et al. [51], and NB mechanism of Sarathy et al. [46] were employed respectively to simulate the premixed flame structure and global characteristics. Table 3 shows some information about the three mechanisms. Sun et al. [34] studied the combustion chemistry of PODE$_3$ firstly and established a high-temperature kinetic mechanism to interpret the laminar premixed combustion, which is similar with the present flame study. The other detailed mechanism constructed by He et al. [47] focused on the ignition characteristic of PODE$_3$ under low to intermediate temperature, which was validated by the rapid compression machine (RCM) ignition and Homogeneous Charge Compression Ignition

(HCCI) experiment. However, He et al. [47] mechanism does not provide the transport data and cannot be used directly as a result. There are six kinetic mechanisms of DMC sequentially proposed by Glaude et al. [48], Hu et al. [49], Sun. et al. [45], Alzueta et al. [50], Alexandrino et al. [51] and Atherley et al. [37]. Mechanisms proposed by Glaude et al., Hu et al. and Alzueta et al. were developed by adding a common DMC sub-mechanism developed by Glaude et al. to different base mechanisms. While, mechanisms proposed by Sun et al. and Alexandrino et al. shared a common DMC sub-mechanism developed by Sun et al. Atherley et al. mechanism was assembled by starting with the updated AramcoMech 3.0 and Alexandrino et al. Atherley et al. conducted the laminar burning speed modeling of the DMC/air mixture using the Glaude et al., Sun et al., and Alexandrino et al. mechanisms, and the order of prediction accuracy of the four mechanisms was: Atherley et al.> Alexandrino et al.> Sun et al.> Glaude et al. However, the Atherley et al. mechanism was not available online. Therefore, in this study, we employed the Alexandrino et al. mechanism for computing the fuel structure of DMC. In general, all the three mechanisms for $PODE_3$, DMC and NB are able to capture the typical reaction classes and pathway of corresponding fuel/air mixture under high-temperature condition, and both of them are validated by well predicting the chemical details for fuel pyrolysis and various flames. Therefore, it is credible to examine the initial fuel cracking process (discussed in *section 4.1.3*) with these mechanisms.

Table 3 Information of the mechanisms used for kinetic analysis

Mechanism	Species	Reaction	Validation	Reference
$PODE_3$ mech	274	1674	Species profile of laminar premixed flame; Laminar burning speed	[34]
DMC mech	497	2737	Ignition delay time (ID) in shock tubes and	[51][45]

			rapid compression machine	
NB mech	118	878	Species profiles in jet stirred reactor (JSR) and opposed-flow diffusion flame; Laminar burning speed	[46]

Numerical study of the laminar premixed flame was performed using the Chemkin Pro package [52]. The flame speed and chemical composition information were computed by the PREMIX code with employing the mixture-averaged transport model and thermal diffusion (Soret effect). The GRID and CURV options were set to 0.05, which allowed the simulation results independent of the grid. This led to solutions approaching 500 grid points. The adiabatic flame temperature (T_{ad}) of fuel/air mixtures were computed with EQUIL code.

4. Result and Discussion

4.1 Laminar burning speed

The laminar burning speed of the three oxygenated fuels were measured over a wide range of equivalence ratios at initial pressure of 0.1 MPa (i.e. ambient pressure) and initial temperature from 363 K to 423 K. First, the present measurements were compared with those in the literature and simulations in order to validate the accuracy of the present approach. Some data in the literature obtained under different conditions from the present work will not be included in the comparison. In general, the measurements concerning the laminar burning speed of n-butanol are ample in the literature, but those for $PODE_3$ and DMC are relatively scare as mentioned in the *introduction section*. These published data in the literature were obtained through different methods, which was more favorable to assess the validity of the current experimental system.

4.1.1 Comparison of the laminar burning speed for PODE$_3$, DMC and NB.

Figure 2(a), (b) and (c) plotted the comparison of our measurements for NB, DMC and PODE$_3$ respectively with the data in literatures as well as simulations. Points represent the measurement results while lines represent the simulation results. Error bars are estimated according to the suggestions in reference [53]. As can be seen from figure 2(a) for NB, our results are in good agreement with those of Zhang et al. [54] at 393 K using spherical flame method, and Knorsch et al. [55] at 423 K using heat flux method. However, our measurements are consistently lower than those of Broustail et al. [56], with an average of 10% for 393 K and 3% for 423 K. Under 423 K, our results are lower than those of Gu et al. [57], which are obtained at 428 K, for lean mixture, but close for stoichiometric and rich mixtures. Compared with the kinetic prediction of Sarathy et al. [46] mechanism, it can be found that for all initial temperatures the mechanism underestimates the laminar burning speed with differences of 7% on average when the equivalence ratio is less than 1.5. Figure 2b plotted the comparison for DMC. For 363 K, the present data are in reasonable agreement with the literature data from Bardin et al. [35] and Atherley et al. [37]. For 423 K, the present data experimental results are still in reasonable agreement with that from Atherley et al. [37] and Yu er al. [36], except for the higher laminar burning speeds for the stoichiometric mixtures. The discrepancy for Φ=1.1 is about 6% comparing with Atherley et al. and 14% comparing with Yu er al. Alexandrino er al. mechanism over-predicts the flame speed on fuel-lean side for both 363 K and 423 K. Figure 2c plotted the comparison of our measurement with the simulated and measured results of Sun et al. [34] at 408 K. In fact, this is the only experimental measurement with respect to the laminar burning speed of PODE$_3$ so far. As can be seen from the comparison, our measurements agree well with the measured and simulated results of Sun et al. [34] for lean and stoichiometric mixture, but lower for rich mixture.

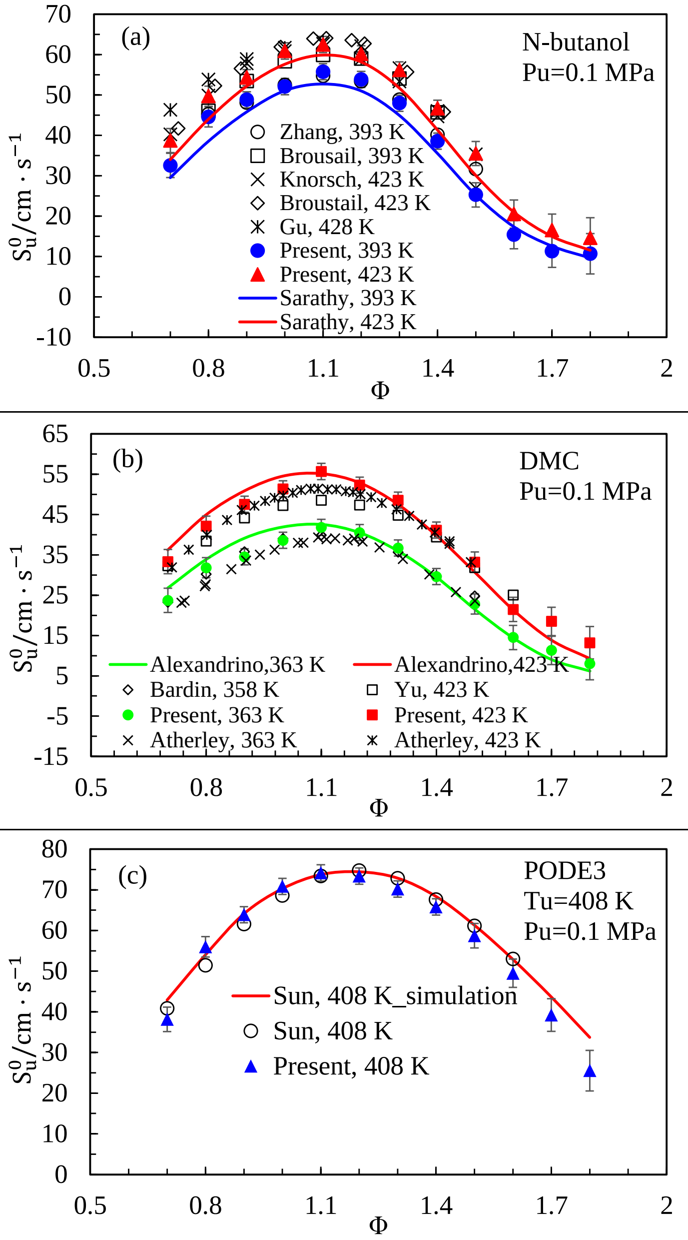

Fig. 2. Laminar burning speed of (a) NB/air mixture, (b) DMC/air mixture and (c) PODE$_3$/air mixture (points are experimental results from present work and literatures; lines are simulated results).

Figure 3 showed the comparison of the laminar burning speeds for NB, DMC and PODE$_3$ at ambient pressure and initial temperature of 393 K. It can be seen from the figure that there are great differences between the laminar burning speeds of the three oxygenated fuels. The laminar burning speed of PODE$_3$ is significantly higher than that of NB and DMC over the whole equivalence ratio range. While, the laminar burning speed of NB is higher than that of DMC for equivalence ratio less than 1.5 and close for equivalence ratio larger than 1.5. The results under other initial temperature conditions also hold the similar trend. Then, the question is what causes the difference in laminar burning speed among the three oxygenated fuels, which will be the topic to be discussed next.

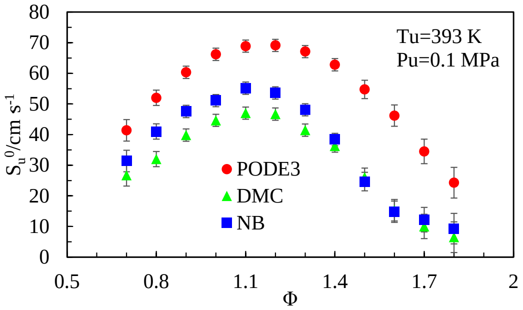

Fig. 3. Comparison of the laminar burning speeds of PODE$_3$, DMC and NB at ambient pressure and initial temperature of 393 K.

4.1.2 Thermal effect

It is generally believed that the adiabatic flame temperature (T$_{ad}$) has a great influence on the laminar burning speed of fuel/air mixture, especially for fuels with similar molecular structure, because it will affect the species equilibrium and the diffusion of heat/radicals into flamefront [18]. Since T$_{ad}$ is directly controlled by the heat of combustion, fuels with larger heats of combustion tend to propagate a flame faster. Fig. 4 plotted the comparison of T$_{ad}$ with respect to PODE$_3$, DMC and NB at atmospheric pressure and 393 K initial temperature. As shown in the figure, T$_{ad}$ of DMC is lower than that of NB and PODE$_3$ over the whole equivalence ratio range, which seems to be consistent with its lowest laminar burning speed among the three. Moreover, although the T$_{ad}$ of PODE$_3$ is higher than that of NB for both lean and rich mixtures, it is close to that of NB for stoichiometric mixture, i.e. the peak value. The comparison about adiabatic flame temperature cannot seem to well explain the fact that the laminar burning speed of $PODE_3$ is obviously higher than that of NB over the whole equivalence ratio range. In order to confirm this viewpoint further, the laminar burning speeds of $PODE_3$ and NB were calculated with nitrogen dilution to such an extent that the adiabatic flame temperature of the respective stoichiometric mixture matched that of the DMC/air mixture. Fig. 5 plotted the comparison of laminar burning speeds of $PODE_3$, NB and DMC with nitrogen dilution. In order to keep the adiabatic flame temperature of stoichiometric mixture consistent, the content of diluted nitrogen was adjusted to 90% for $PODE_3$, 88% for NB and 79% for DMC, i.e. air. It can be seen from the figure that although the adiabatic flame temperature keeps the same, the laminar burning speed of $PODE_3$ is still significantly higher than that of NB and DMC. Interestingly, the laminar burning speed of NB is lower than that of DMC when keeping the same adiabatic flame temperature, which is contrary to the result in Fig. 3. This result implies that the adiabatic flame temperature is not the only dominant factor of laminar flame velocity for oxygenated fuels, which leads us to check the possible kinetic effect caused by different molecular structure, discussed next.

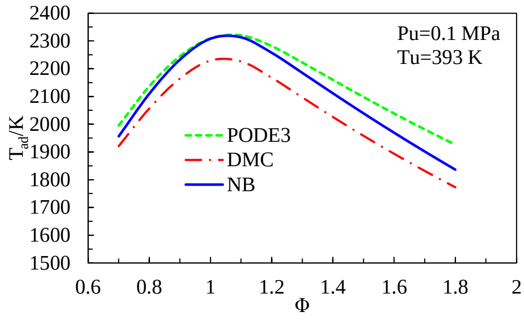

Fig. 4. Comparison of the adiabatic flame temperatures of $PODE_3$/air, DMC/air and NB/air mixture at ambient pressure and 393 K initial temperature.

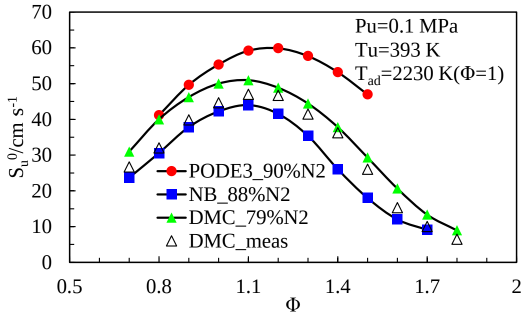

Fig. 5. Comparison of the laminar burning speeds of $PODE_3$, DMC and NB with nitrogen dilution.

4.1.3 Kinetic effect

Since the three mechanisms used above, namely Sun et al. [34] mechanism for $PODE_3$, ~~Sun~~ Alexandrino et al. [51] mechanism for DMC and Sarathy et al. [46] mechanism for NB, predicted respective laminar burning speed with an acceptable accuracy as showed in Fig. 3, it is therefore reasonable to use them for investigating the kinetic effect subsequently.

Firstly, the sensitivity analysis was carried out to determine the reaction pathway that dominates the flame propagation. The normalized sensitivity coefficient is given by the following formula:

$$K_i = \frac{A_i}{S_u^0}\frac{\alpha S_u^0}{\alpha A_i} \tag{7}$$

where A_i is the pre-exponential factor of reaction i. It is recognized that reactions with high sensitivity on laminar burning speed are rate limiting. Fig. 6a, b, c plotted the normalized sensitivity coefficient for $PODE_3$, DMC and NB respectively at atmospheric pressure, 393K initial temperature and various equivalence ratios. Fuel-specific reactions and those different from other fuels were highlighted for each fuel. As seen from the figure, it is the reactions involving small species (C_0-C_1) that dominate the burning rate, except for the individual fuel-specific reactions for rich mixtures. This law is consistent with hydrocarbons [19-23], which indicating that there is no fundamental difference between the kinetic of oxygenates with that of hydrocarbons. The top three positive sensitivity reactions for both the three oxygenates are the chain-branching reactions: H+O$_2$=OH+O, CO+OH=CO$_2$+H, and decomposition of HCO: HCO+M=H+CO+M. While the chain termination reactions such as R9 for PODE$_3$, R9 for DMC and R8, R9 for NB exhibit a negative influence on the flame propagation. Some fuel-related reactions (R14, R16) of DMC produce an effect for rich mixture. The sensitivity response of NB is quite different from that of PODE$_3$ and DMC, that is, many reactions involving C$_2$-C$_4$ fuel fragments exhibit a certain degree of sensitivity, although lower than that of small species reactions, to the burning rate. It is related to the fact that NB contains a long alkyl group (C$_4$), while PODE$_3$ and DMC have no C-C bond.

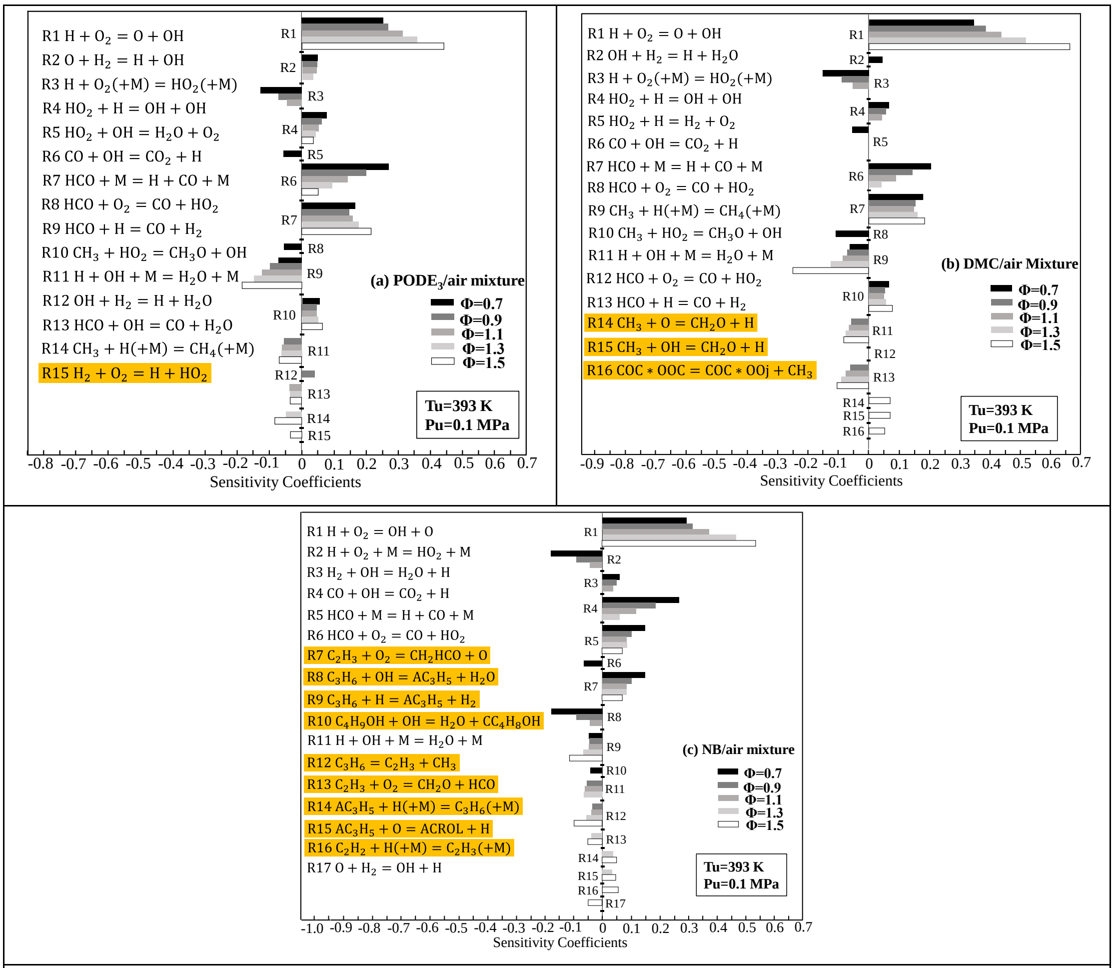

Fig. 6. Sensitivity analysis of laminar burning speed for PODE$_3$, DMC and NB, Φ=0.7-1.5, Pu=0.1 MPa and Tu=393 K (the major different reactions from other fuels are highlighted in

yellow).

From the analysis above, it can be concluded that C_0-C_1 species (oxygenated or not) in the reaction zone have a significant impact on the laminar burning speed. Therefore, we further examine the profiles of C_0-C_1 species in the flame structures, as showed in Fig. 7. All of these species participate in the important sensitivity reactions of the three fuels. As can be seen from the figure, CO, H, O, OH showed in Fig.7(a) have a dominated concentration when compared with the CH_x species showed in Fig.7(b). Considering these dominated species further, it can be seen that the mole fractions of CO, H, O, OH and HO_2 for $PODE_3$ are significantly higher than those for DMC and NB. This is consistent with the results that the laminar burning speed of $PODE_3$ is significantly higher than that of the other two fuels. By comparison, the difference between DMC and NB is less significant. Specifically, the mole fractions of H, O and CO for DMC are higher than those for NB by 10.7%, 4.4% and 11.9% respectively, while the mole fractions of OH and HO_2 for NB are higher than those for DMC by 9.9% and 21.0% respectively. In addition, the mole fraction of CH_3 and HCO for DMC is respective twice and 2.4 times of that for NB, which is attributed to the fuel-specific decomposition pathway, as discussed next. In summary, both thermal effect and kinetic effect show evidence for the highest laminar burning speed of $PODE_3$ among the three, while the higher flame speed of NB than that of DMC is the combined effect of thermal factor and kinetic factor.

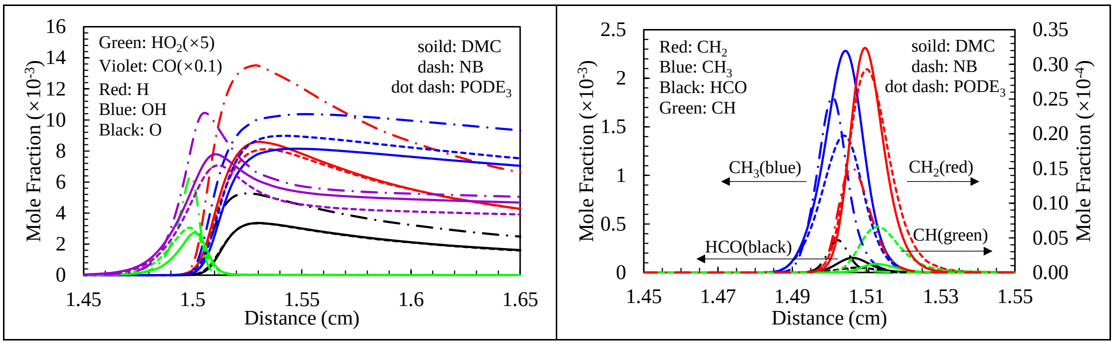

Fig. 7. Simulated mole fraction profiles of major C_0–C_1 intermediates in the flame of $PODE_3$, DMC and NB, Φ=1.0., Pu=0.1 MPa and Tu=393 K.

Although it is the small species reactions that dominate the global heat release and flame propagation, the initial fuel cracking forms fuel fragments and intermediates with different reactivity, which provides a prerequisite for the subsequent small species reactions, as Wu et al. [24] commented. While these fuel cracking processes are completely fuel-specific reactions due to the different fuel molecular structure. By considering the bond energy, Wu et al. [24] has unified the alcohol fuel with the hydrocarbon fuel, because the bond energy of C-C bond is similar to that of C-O bond, while the bond energy of C-H bond is similar to that of O-H bond. Therefore, a more general conclusion is drawn, that is, the flame speed of branched fuel is slower than that of straight-chain fuel, which is applicable to both hydrocarbons and alcohols. Now, we examine this generality for $PODE_3$ and DMC. Fig. 8 showed the dissociation bond energies of $PODE_3$, DMC and NB, which are referred to the study of Sun et al. [34], Glaude et al. [48] and Gu et al. [32], respectively. They are all calculated by Gaussian code [58], which allows comparison between different fuels. As can be seen from the figure, there is no C-C bond in $PODE_3$ and DMC, but the bond energy of C-O bond is similar to that of C-C and C-O bond in NB, except for higher bond energy of C-O linked to the inner C in DMC. In this sense, $PODE_3$ can be regarded as a straight-chain C_9 molecule, NB as a straight-chain C_5 molecule, while DMC as a branched structure because there exists a branched C=O bond.

Detailed reaction pathway analysis of the three oxygenated fuels in low-pressure premixed flame have been conducted in the previous studies ([34] for $PODE_3$, [45] for DMC and [24] for NB). In the present study, a few reaction steps were extracted in order to highlight the initial cracking process of the three fuels (see Fig. S4). For both the three, H-abstraction following by β-scission is the dominant path for initial fuel consumption. H-abstraction for $PODE_3$ is mainly from the CH_3O moieties and the formed fuel radical DMM3A [$CH_3O(CH_2O)_3CH_2$] is almost entirely decomposed in the formaldehyde (CH_2O) through a series of β-scission from C-O bonds. Similarly, H-abstraction from DMC generates fuel radical $CH_3OC(=O)OCH_2$ which decomposes into CH_3OCO and CH_2O by β-scission. Then, CH_3OCO continue to decompose into CO_2 and CH_3. Actually, CH_2O was experimentally detected with a remarkable mole concentration from both $PODE_3$ flame [34] and DMC flame [45]. The highly reactive CH_2O participates in the chain-branching reactions to form HCO ($CH_2O+O=HCO+OH$, $CH_2O+OH=HCO+H_2O$, $CH_2O+H=HCO+H_2$), as shown from the Rate of Production (ROP) analysis of CH_2O in $PODE_3$ flame conducted by Sun et al. [34]. This explains why the mole fraction of HCO in the $PODE_3$ flame is 2.7 times of that for DMC and 6.5 times of that for NB (as shown in Fig. 7). Further, as identified by the sensitivity analysis shown in Fig. 6, HCO is related to one of three most sensitive reactions dominating flame propagation. The initial cracking of NB form fuel fragments such as alkenes, enols, smaller alcohols and ketones, which is significantly different from that of $PODE_3$ and DMC due to the relatively large alkyl within NB versus the absence of C-C bond within $PODE_3$ and DMC.

(a)	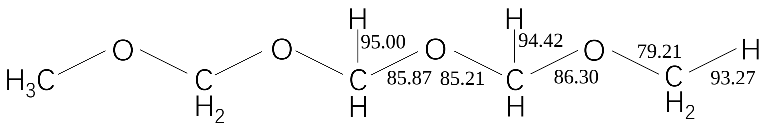
(b)	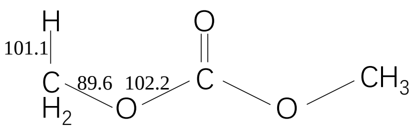

(c)

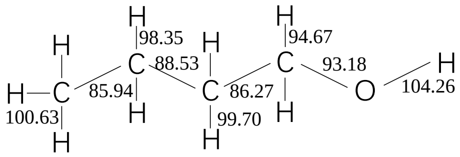

Fig. 8. Bond dissociation energies BDEs of PODE$_3$, DMC and NB (unit: kcal/mol).

4.2 Markstein length

The Markstein length (L_b), quantifying the sensitivity of flame speed to the variation of flame stretch ratio, is an important parameter to characterize the effect of stretch on global flame instability. Positive L_b means a stable flame while negative means an unstable flame. Fig. 9 depicted the Markstein lengths versus equivalence ratio Φ for the three fuels at ambient pressure and 393 K initial temperature. These values were obtained from the extrapolation with NM1 as shown in Eq. (4). As can be seen from the figure, for both of the three oxygenates, L_b decreases with equivalence ratio and changes from positive to negative as $\Phi>1.3$. This trend is similar to that of previous studies with respect to NB [24,32] and hydrocarbons [59]. It is indicated that the flame gradually loses its stability with the increase of equivalence ratio. When compared different fuels, closed Markstein lengths for the three fuels are observed when $\Phi\leq1.3$, while obvious discrepancies between the three appear when $\Phi>1.3$. PODE$_3$ has the highest Markstein length among the three following by NB and DMC in order. When examining the Markstein number (M_a) (as shown in Fig. 10) which is the Markstein length scaled by flame thickness (l_f), the order does not seem to have changed much. Specifically, PODE$_3$ has a significantly higher Markstein number than DMC and NB for $\Phi\leq1.3$ and a much closer one for $\Phi>1.3$. While, the discrepancy between Markstein number of NB and DMC increases for $\Phi>1.3$. This is because the flame thickness of the three fuels follows the order of NB>DMC>PODE$_3$ as shown in Fig. 11. It is implied that PODE$_3$ has a more stable flame behavior in global perspective following by NB and DMC in order.

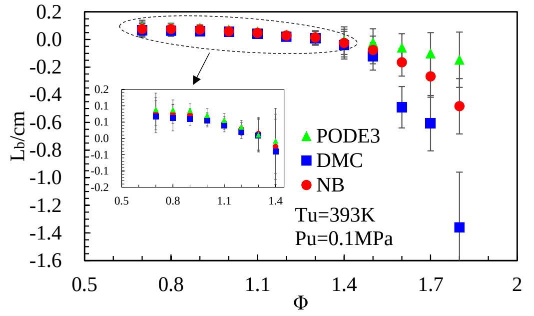

Fig. 9. Markstein lengths versus equivalence ratio for PODE$_3$, DMC and NB at ambient pressure and 393 K initial temperature.

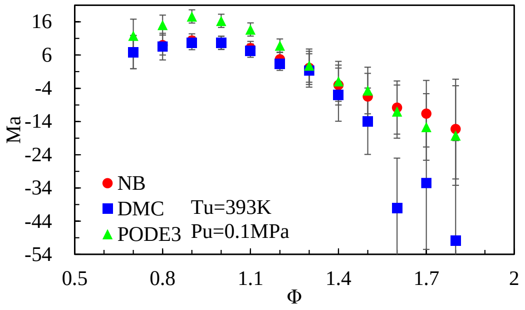

Fig. 10. Markstein numbers versus equivalence ratio for PODE$_3$, DMC and NB at ambient pressure and 393 K initial temperature.

4.3 Flame instability

Laminar flame is naturally subjected to the instability effect even without external disturbances. This instability is caused by three factors, namely buoyancy instability, diffusive-thermal instabilities and hydrodynamic instability, among which the latter two are the main ones [18]. It is expected that different fuels have different flame instability tendencies because they have different transport and flow characteristics. Therefore, in this section, we will compare the characteristics of cellular instability of PODE$_3$, DMC and NB.

According to the theory of flame instability, diffusive-thermal instabilities is caused by the nonequidiffusion effect between the thermal diffusivity and mass diffusivity. This can be characterized by the Lewis number (Le), which is defined as the ratio of the thermal diffusivity to the mass diffusivity of the deficient reactant, given by Eq. (8),

$$Le = \frac{\lambda/C_p}{\rho D} \tag{8}$$

where λ (W•m^{-1}•K^{-1}) is the thermal conductivity, C_p (J•Kg^{-1}•K^{-1}) and ρ are the specific heat and density of unburned gas respectively, D is the mass diffusion coefficient of deficient reactant which refers to fuel for lean mixture and oxidizer for rich mixture. It has been well recognized that diffusion helps to stabilize the flame when Le>1 and leads to flame instability otherwise. The hydrodynamic instability is caused by the density jump across the flame surface and can be characterized by thermal expansion ratio: $\sigma = \rho_u/\rho_b$, where ρ_u and ρ_b are the density of unburned gas and burned gas respectively. Flame thickness (L_f) can also exert an influence on the hydrodynamic instability through the density gradient. Increasing σ and decreasing L_f lead to enhancing hydrodynamic instability. There are two popular definitions for flame thickness, one based on the kinetic analysis (Eq. (9)) and the other based on gradient method (Eq. (10)). T_{ad}, T_u and $(dT/dx)_{max}$ in Eq. (10) are the adiabatic flame temperature, initial temperature and the maximum temperature gradient respectively.

$$L_f = \frac{\lambda}{\rho_u C_p S_u^0} \tag{9}$$

$$L_f = \frac{T_{ad} - T_u}{(dT/dx)_{max}} \tag{10}$$

Both of the definitions were employed to determine the flame thickness of the three oxygenated fuels and the results comparison was showed in Fig. S5. The L_f in this section is determined by Eq. (10) to avoid the uncertainty of Eq. (9) caused by the arbitrariness of the temperature at which λ/C_p is assessed.

Tests for lean mixture under low initial pressure failed to identified the onset of cellular instability because of the narrow visualization scope of the present vessel. Therefore, the tests for comparing the propensity to destabilize of different fuels were conducted at the initial conditions favoring the onset of cellular instability, i.e. large equivalence ratio and high pressure. Fig. 11 showed the schlieren photographs for flame propagation of the three oxygenates at initial temperature of 393 K, equivalence ratio of 1.5 and initial pressure of 0.5 MPa (Fig. 11(a)) and 0.75 MPa (Fig. 11(b)). The instantaneous flame radii R_f were marked on the left side, which were deduced through calculating the area of the flame ragion as mentioned in *Section 2.2*. Parameters (L_f, σ, Le) related to flame instability were listed in the bottom of the figure. As can be seen from the Fig. 11(a), at the beginning of the propagation the flame remains basically smooth, and then cracks appear on the flamefront following by branching and losing similarity. From a certain moment on, cellular structure appears spontaneously and gradually covers the whole flame surface. This is a typical formation process of cellular instability for premixed laminar flame. When compared the propensity to destabilize of different fuels, no cells are observed in the flame of $PODE_3$/air mixture for the duration of observation, which is completely different from that of the flames fueled DMC and NB. That implies a more stable flame for $PODE_3$ than that for DMC and NB. In fact, the cellular structure of the $PODE_3$/air flame was observed as the flame edge out of sight (see Fig. S6), which indicates that a larger visual window and hence longer observation time are needed to determine to onset of instability for $PODE_3$. When comparing the instability prameters, the three oxygenates have a close σ and Le, while the L_f for $PODE_3$ is smaller than that of DMC and NB, which seems to imply a stronger hydrodynamic instability. However, the more stable flame of $PODE_3$ can be explained by the larger stratch rate recognizing that positive stretch in outwardly propagating flame has been found to stabilize the flame and suppress the cellular instability at a result. Under certain flame radius the fester flame speed for $PODE_3$ against DMC and NB causes a lager flame stratch rate due to the the positive correlation between the flame speed and stratch rate as shown in Eq.(2).

DMC flame and NB flame have an approximately similar flame intability characteristic from the flame morphology. For Pu=0.5 MPa, an earlier onset of instability is observed for DMC/air mixture when compared to that of NB flame. This indiates a more stable flame for NB against that for DMC, which is also supported by both the diffusive-thermal factor (Le) and hydrodynamic factor (σ, L_f). While, at Pu=0.75 MPa, DMC and NB seem to have a closer flame instability behavior.

<table>
<tr><td></td><td colspan="3">(a) 0.5 MPa</td><td colspan="3">(b) 0.75 MPa</td></tr>
<tr><td>8 cm</td><td colspan="6" rowspan="5">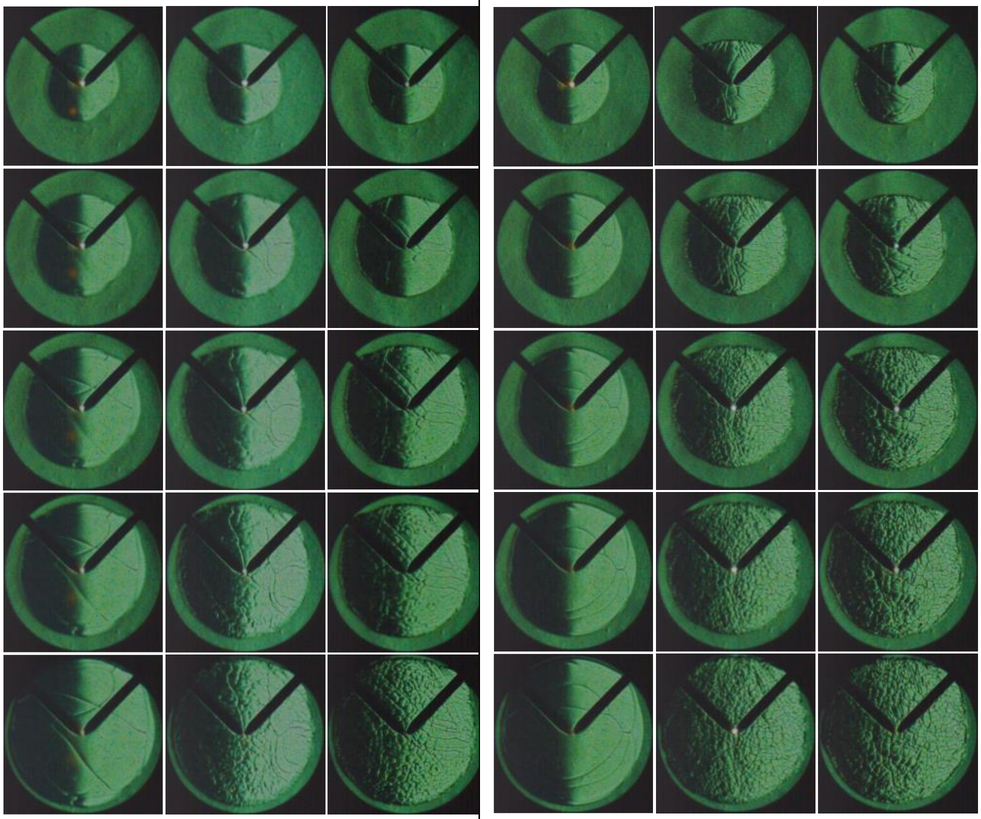</td></tr>
<tr><td>12 cm</td></tr>
<tr><td>16 cm</td></tr>
<tr><td>20 cm</td></tr>
<tr><td>24 cm</td></tr>
<tr><td>Fuel</td><td>PODE$_3$</td><td>NB</td><td>DMC</td><td>PODE3</td><td>NB</td><td>DMC</td></tr>
<tr><td>l_f/mm</td><td>0.0130</td><td>0.0194</td><td>0.0185</td><td>0.0112</td><td>0.0172</td><td>0.0164</td></tr>
<tr><td>σ</td><td>6.90</td><td>6.38</td><td>6.58</td><td>6.98</td><td>6.40</td><td>6.62</td></tr>
<tr><td>Le</td><td>0.883</td><td>0.973</td><td>0.872</td><td>0.884</td><td>0.975</td><td>0.871</td></tr>
<tr><td colspan="7">Fig. 11. Schlieren photographs for flame propagation of PODE$_3$, DMC and NB, Φ=1.5, Tu=393 K and Pu=0.5, 0.75 MPa.</td></tr>
</table>

Flame instability can be quantified by the critical radius (R_{cr}) describing the onset of cellular instability and critical Peclet number (Pe_{cr}), dimensionless R_{cr} scaled by flame thickness. The R_{cr} at present work was determined based on the second defination of Bradley et al.[41], which refers to the instant when the cells spontaneously cover the whole flame surface. The uncertainty in meauring R_{cr} is about 8-12% arising mainly from the finite framing rate in capturing the instant of transition. Fig. 12 showed R_{cr} and corresponding Pe_{cr} versus equivalence ratio for DMC and NB at 0.75 MPa. As can be seen from the figure, although the R_{cr} for NB is consistent smaller than that for DMC, the difference is actually less than 3% which is lower than the experimental uncertainty. Similarly, the Pe_{cr} for DMC and NB is also close with the biggest difference of 10%.

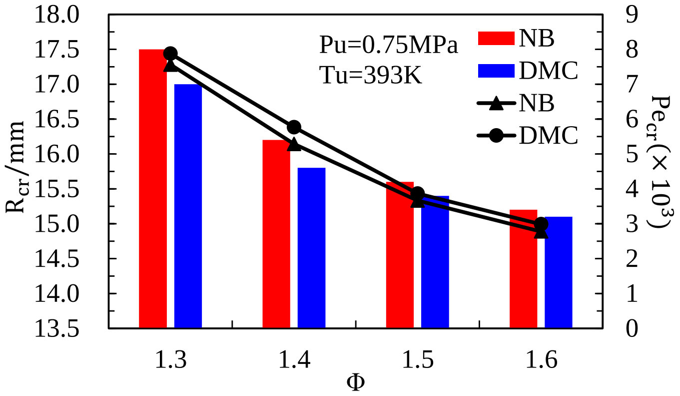

Fig. 12. Critical radius and Peclet number versus equivalence ratio for DMC and NB at 0.75 MPa.

Conclusion

Laminar burning speed, Markstein length and cellular Instability of PODE$_3$, DMC and NB mixtures with air were experimentally studied using spherical propagation flame method. Laminar burning speeds and Markstein lengths were measured at ambient pressure and elevated temperatures from 363 K to 423 K over a wide range of equivalence ratios, while flame instabilities were studied at high pressure (0.5-0.75 MPa). Three models including linear and non-linear extrapolation were employed to extract unstretched flame speed and Markstein lengths of oxygenated fuels and the performances were compared. Computed flame structure with well-validated kinetic mechanisms of the three fuels respectively were employed to examine the thermal effect and kinetic effect governing the flame propagation of oxygenated fuels and understand the underlying effect of the molecular structure of oxygenated fuels on laminar flame propagation. Onset of flame cellular instability was determined for the three fuels.

Results show that under the same initial conditions, unstretched flame speed exacted by LM has the highest value following by NM2 and NM1. The difference between the extracted flame speeds and Markstein lengths by the three models increases for over-rich mixtures ($\Phi \geq 1.6$) and lean mixtures ($\Phi \leq 0.9$). PODE$_3$ has the highest laminar burning speed among the three following by NB and DMC in order; with the burning speed of PODE$_3$ being significantly higher than that of DMC and NB~~.~~ Both thermal effect and kinetic effect support the highest laminar burning speed of PODE$_3$ among the three fuels; while the higher flame speed of NB than that of DMC is the combined effect of thermal factor and kinetic factor.

Molecular structure of oxygenated fuels exerts an influence on the laminar flame propagation through the fuel-specific cracking pathway and resulting formed intermediates with different reactivity. Due to no C-C bond within the molecular of PODE$_3$ and DMC, substantial oxy-intermediates (CH_2O) with high reactivity are formed during fuel decomposition. The C-O bonds energy in PODE3 and DMC is comparable to that of C-C bond and C-O bond in NB, and these bonds play a same role in fuel decomposition reaction, especially for β-scission. This seems to extend the rule that the role of an O atom is similar to a C atom when considering the fuel molecular structure. More efforts are need to confirm this generalization by examining more other ethers and esters as well as oxygenates with other functional group.

Both the Markstein lengths and flame morphology suggest a more stable flame for PODE$_3$/air mixture following by NB and DMC in order. This is due to the strong stretching of PODE$_3$, which is beneficial to suppress the cellular instability for outwardly spherical flame. The flame stability of DMC and NB is approximately similar especially at high initial pressure. The differences between the critical radius R_{cr} and Peclet number Pe_{cr} for DMC and NB are less than 3% and 10% respectivly, which is lower than the exipermental uncertainty.

Acknowledgments

This research is supported by National Natural Science Foundation of China (Project code: 51476069, 51676084); Jilin Provincial Industrial Innovation Special Guidance Fund Project (Project code: 2019C058-3); Jilin Province Science and Technology Development Plan Project (Project code: 20180101059JC); Jilin Province Specific Project of Industrial Technology Research & Development (Project code: 2020C025-2). The authors gratefully acknowledge Sun. W and co-workers for their PODEn mechanism and DMC mechanism, and Sarathy. M and co-workers for their n-butanol mechanism.

Reference

[1] British Petroleum Company (BP). BP energy outlook 2019. London; 2019.

[2] Noh HK, No SY. Effect of bioethanol on combustion and emissions in advanced CI engines: HCCI, PPC and GCI mode – A review. Applied Energy 2017; 208:782-802.

[3] Bergthorson JM, Thomson MJ. A review of the combustion and emissions properties of advanced transportation biofuels and their impact on existing and future engines. Renewable

and Sustainable Energy Reviews 2015; 42:1393-1417.

[4] Omar IA, Mamat R, Ibrahim TK, Hammid AT, Yusri IM, Hamidi MA, et al. Overview of the oxygenated fuels in spark ignition engine: Environmental and performance. Renewable and Sustainable Energy Reviews 2018; 91:394-408.

[5] Verma P, Jafari M, Rahman SMA, Pickering E, Stevanovic S, Dowell A, et al. The impact of chemical composition of oxygenated fuels on morphology and nanostructure of soot particles. Fuel 2019; 259:116167.

[6] Liu HY, Wang Z, Li YF, Zheng YY, He TJ, Wang JX. Recent progress in the application in compression ignition engines and the synthesis technologies of polyoxymethylene dimethyl ethers. Applied Energy 2019; 233:599-611.

[7] Abdalla AOG, Liu D. Dimethyl Carbonate as a Promising Oxygenated Fuel for Combustion: A Review. Energies 2018; 11(6):1552-1572.

[8] Trindade WRD, dos Santos RG. Review on the characteristics of butanol, its production and use as fuel in internal combustion engines. Renewable and Sustainable Energy Reviews 2017; 69:642-651.

[9] No SY. Application of biobutanol in advanced CI engines – A review. Fuel 2016; 183:641-658.

[10] Wang Z, Liu HY, Ma X, Wang JX, Shuai SJ, Reitz RD. Homogeneous charge compression ignition (HCCI) combustion of polyoxymethylene dimethyl ethers (PODE). Fuel 2016; 183:206-213.

[11] Liu HY, Wang Z, Zhang J, Wang JX, Shuai SJ. Study on combustion and emission characteristics of Polyoxymethylene Dimethyl Ethers/diesel blends in light-duty and heavy-duty diesel engines. Applied Energy 2017; 185:1393-1402.

[12] Liu JL, Shang HY, Wang H, Zheng ZQ, Wang QP, Xue ZZ, et al. Investigation on partially premixed combustion fueled with gasoline and PODE blends in a multi-cylinder heavy-duty diesel engine. Fuel 2017; 193:101-111.

[13] Pan MZ, Qian WW, Zheng ZY, Huang R, Zhou XR, Huang HZ, et al. The potential of dimethyl carbonate (DMC) as an alternative fuel for compression ignition engines with different EGR rates. Fuel 2019; 257:115920.

[14] Kumar BR, Saravanan S. Partially premixed low temperature combustion using dimethyl carbonate (DMC) in a DI diesel engine for favorable smoke/NOx emissions. Fuel 2016; 180:396-406.

[15] Tan YR, Botero ML, Sheng Y, Dreyer JAH, Xu R, Yang WM, et al. Sooting characteristics of polyoxymethylene dimethyl ether blends with diesel in a diffusion flame. Fuel 2018; 224:499-506.

[16] Yang JC, Jiang Y, Karavalakis G, Johnson KC, Kumar S, Cocker DR, et al. Impacts of dimethyl carbonate blends on gaseous and particulate emissions from a heavy-duty diesel engine. Fuel 2016; 184:681-688.

[17] Egolfopoulos FN, Hansen N, Ju Y, Kohse-Höinghaus K, Law CK, Qi F. Advances and challenges in laminar flame experiments and implications for combustion chemistry. Progress in Energy and Combustion Science 2014; 43:36-67.

[18] Law CK. Combustion physics. Cambridge University Press; 2010.

[19] DAVIS SG, LAW CK. Determination of and Fuel Structure Effects on Laminar Flame Speeds of C1 to C8 Hydrocarbons. Combustion Science and Technology 1998; 140:427-449.

[20] Kelley AP, Smallbone AJ, Zhu DL, Law CK. Laminar flame speeds of C5 to C8 n-alkanes at

elevated pressures: Experimental determination, fuel similarity, and stretch sensitivity. Proceedings of the Combustion Institute 2010; 33(1):963-970.

[21] Ji CS, Dames E, Wang YL, Wang H, Egolfopoulos FN. Propagation and extinction of premixed C5–C12 n-alkane flames. Combustion and Flame 2010; 157(2):277-287.

[22] Mehl M, Herbinet O, Dirrenberger P, Bounaceur R, Glaude PA, Battin-Leclerc F, et al. Experimental and modeling study of burning velocities for alkyl aromatic components relevant to diesel fuels. Proceedings of the Combustion Institute 2015; 35(1):341-348.

[23] Wu FJ, Kelley AP, Law CK. Laminar flame speeds of cyclohexane and mono-alkylated cyclohexanes at elevated pressures. Combustion and Flame 2012; 159(4):1417-1425.

[24] Wu FJ, Law CK. An experimental and mechanistic study on the laminar flame speed, Markstein length and flame chemistry of the butanol isomers. Combustion and Flame 2013; 160(12):2744–2756.

[25] Law CK, Sung CJ. Structure, aerodynamics, and geometry of premixed flamelets. Progress in Energy and Combustion Science 2000; 26:459-505.

[26] Law CK, Jomaas G, Bechtold JK. Cellular instabilities of expanding hydrogen/propane spherical flames at elevated pressures: Theory and experiment. Proceedings of the Combustion Institute 2005; 30(1):159-167.

[27] Kwon OC, Rozenchan G, Law CK. Cellular instabilities and self-acceleration of outwardly propagating spherical flames. Proceedings of the Combustion Institute 2002; 29(2):1775-1783.

[28] Wu FJ, Jomaas G, Law CK. An experimental investigation on self-acceleration of cellular spherical flames. Proceedings of the Combustion Institute 2013; 34(1):937-945.

[29] Okafor EC, Nagano Y, Kitagawa T. Experimental and theoretical analysis of cellular instability

in lean H2-CH4-air flames at elevated pressures. International Journal of Hydrogen Energy 2016; 41(15):6581-6592.

[30] Kim HJ, Van K, Lee DK, Yoo CS, Park J, Chung SH. Laminar flame speed, Markstein length, and cellular instability for spherically propagating methane/ethylene–air premixed flames. Combustion and Flame 2020; 214:464-474.

[31] Liu FS, Liu ZC, Sang Z, He X, Sjöberg M, Vuilleumier D, et al. Numerical study and cellular instability analysis of E30-air mixtures at elevated temperatures and pressures. Fuel 2020; 271:117458.

[32] Gu XL, Huang ZH, Wu S, Li QQ. Laminar burning velocities and flame instabilities of butanol isomers–air mixtures. Combustion and Flame 2010; 157(12):2318-2325.

[33] Beeckmann J, Cai L, Pitsch H. Experimental investigation of the laminar burning velocities of methanol, ethanol, n-propanol, and n-butanol at high pressure. Fuel 2014; 117:340-350.

[34] Sun WY, Wang GQ, Li S, Zhang RZ, Yang B, Yang JZ, et al. Speciation and the laminar burning velocities of poly (oxymethylene) dimethyl ether 3 (POMDME3) flames: An experimental and modeling study. Proceedings of the Combustion Institute 2017; 36(1):1269–1278.

[35] Bardin ME, Ivanov EV, Nilsson EJK, Vinokurov VA, Konnov AA. Laminar Burning Velocities of Dimethyl Carbonate with Air. Energy & Fuels 2013; 27(9):5513-5517.

[36] Yu HB, Hu EJ, Yang K, Huang ZH. Experimental and Numerical Research on Laminar Burning Characteristics of Premixed Dimethyl Carbonate/Air Flames. Journal of Xi'an Jiaotong University 2014; 48(11):25-31.

[37] Atherley T, Persis S, Chaumeix N, Fernandes Y, Bry A, Comandini A, et al. Laminar flame speed and shock-tube multi-species laser absorption measurements of Dimethyl Carbonate

oxidation and pyrolysis near 1 atm. Proceedings of the Combustion Institute, https://doi.org/10.1016/j.proci.2020.06.333

[38] Burke MP, Chen Z, Ju YG, Dryer FL. Effect of cylindrical confinement on the determination of laminar flame speeds using outwardly propagating flames. Combustion and Flame 2009; 156(4):771-779.

[39] Mannaa O, Mansour MS, Roberts WL, Chung SH. Laminar burning velocities at elevated pressures for gasoline and gasoline surrogates associated with RON. Combustion and Flame 2015; 162(6):2311-2321.

[40] Kelley AP, Law CK. Nonlinear effects in the extraction of laminar flame speeds from expanding spherical flames. Combustion and Flame 2009; 156(9):1844-1851.

[41] Bradley D, Hicks RA, Lawes M, Sheppard CGW, Woolley R. The measurement of laminar burning velocities and Markstein numbers for iso-octane–air and iso-octane–n-heptane–air mixtures at elevated temperatures and pressures in an explosion bomb. Combust and Flame 1998; 115:126-144.

[42] Chen Z, Burke MP, Ju YG. Effects of Lewis number and ignition energy on the determination of laminar flame speed using propagating spherical flames. Proceedings of the Combustion Institute 2009; 32:1253-1260.

[43] Chen Z. On the extraction of laminar flame speed and Markstein length from outwardly propagating spherical flames. Combustion and Flame 2011; 158(2):291-300.

[44] Wu FJ, Liang WK, Chen Z, Ju YG, Law CK. Uncertainty in stretch extrapolation of laminar flame speed from expanding spherical flames. Proceedings of the Combustion Institute 2015; 35(1):663-670.

[45] Sun WY, Yang B, Hansen N, Westbrook CK, Zhang F, Wang G, et al. An experimental and kinetic modeling study on dimethyl carbonate (DMC) pyrolysis and combustion. Combustion and Flame 2016; 164:224–238.

[46] Sarathy SM, Thomson MJ, Togbé C, Dagaut P, Halter F, Mounaim-Rousselle C. An experimental and kinetic modeling study of n-butanol combustion. Combustion and Flame 2009; 156(4):852-864.

[47] He TJ, Wang Z, You XQ, Liu HY, Wang YD, Li XY, et al. A chemical kinetic mechanism for the low- and intermediate-temperature combustion of Polyoxymethylene Dimethyl Ether 3 (PODE3). Fuel 2018; 212:223-235.

[48] Glaude PA, Pitz WJ, Thomson MJ. Chemical kinetic modeling of dimethyl carbonate in an opposed-flow diffusion flame. Proceedings of the Combustion Institute 2005; 30:1111–1118.

[49] Hu EJ, Chen YZ, Zhang ZH, Pan L, Li QQ, Cheng Y, et al. Experimental and kinetic study on ignition delay times of dimethyl carbonate at high temperature. Fuel 2015; 140:626–632.

[50] Alzueta MU, Salinas P, Millera A, Bilbao R, Abian M. A study of dimethyl carbonate conversion and its impact to minimize soot and NO emissions. Proceedings of the Combustion Institute 2016; 36(3):3985-3993.

[51] Alexandrino K, Alzueta MU, Curran HJ. An experimental and modeling study of the ignition of dimethyl carbonate in shock tubes and rapid compression machine. Combustion and Flame 2018; 188:212-226.

[52] CHEMKIN-PRO 15112, Reaction Design, San Diego, 2012.

[53] Chen Z. On the accuracy of laminar flame speeds measured from outwardly propagating spherical flames: Methane/air at normal temperature and pressure. Combustion and Flame

2015; 162(6):2442-2453.

[54] Zhang XY, Tang CL, Yu HB, Li QQ, Gong J, Huang ZH. Laminar Flame Characteristics of iso-Octane/n-Butanol Blend-Air Mixtures at Elevated Temperatures. Energy & Fuels 2013; 27(4):2327-2335.

[55] Knorsch T, Zackel A, Mamaikin D, Zigan L, Wensing M. Comparison of Different Gasoline Alternative Fuels in Terms of Laminar Burning Velocity at Increased Gas Temperatures and Exhaust Gas Recirculation Rates. Energy & Fuels 2014; 28(2):1446–1452.

[56] Broustail G, Seers P, Halter F, Moréac G, Mounaim-Rousselle C. Experimental determination of laminar burning velocity for butanol and ethanol iso-octane blends. Fuel 2011; 90(1):1-6.

[57] Gu XL, Huang ZH, Li QQ, Tang CL. Measurements of Laminar Burning Velocities and Markstein Lengths of n-Butanol Air Premixed Mixtures at Elevated Temperatures and Pressures. Energy & Fuels 2009; 23(5):4900-4907.

[58] Curtiss LA, Redfern PC, Raghavachari K. Gaussian-4 theory. Journal of Chemical Physics 2007; 126(8):084108.

[59] Galmiche B, Halter F, Foucher F. Effects of high pressure, high temperature and dilution on laminar burning velocities and Markstein lengths of iso-octane/air mixtures. Combustion and Flame 2012; 159(11):3286-3299.